AIP | Physics of Plasmas

Collective focusing of intense ion beam pulses for high-energy density physics applications

Mikhail A. Dorf, Igor D. Kaganovich, Edward A. Startsev, and Ronald C. Davidson

Citation: Phys. Plasmas **18**, 033106 (2011); doi: 10.1063/1.3557894

View online: http://dx.doi.org/10.1063/1.3557894

View Table of Contents: http://pop.aip.org/resource/1/PHPAEN/v18/i3

Published by the American Institute of Physics.

Collective focusing of intense ion beam pulses for high-energy density physics applications

Mikhail A. Dorf,[a] Igor D. Kaganovich, Edward A. Startsev, and Ronald C. Davidson
Plasma Physics Laboratory, Princeton, New Jersey 08543, USA

(Received 1 October 2010; accepted 31 January 2011; published online 24 March 2011)

The collective focusing concept in which a weak magnetic lens provides strong focusing of an intense ion beam pulse carrying a neutralizing electron background is investigated by making use of advanced particle-in-cell simulations and reduced analytical models. The original analysis by Robertson [Phys. Rev. Lett. **48**, 149 (1982)] is extended to the parameter regimes of particular importance for several high-energy density physics applications. The present paper investigates (1) the effects of non-neutral collective focusing in a moderately strong magnetic field; (2) the diamagnetic effects leading to suppression of the applied magnetic field due to the presence of the beam pulse; and (3) the influence of a finite-radius conducting wall surrounding the beam cross-section on beam neutralization. In addition, it is demonstrated that the use of the collective focusing lens can significantly simplify the technical realization of the final focusing of ion beam pulses in the Neutralized Drift Compression Experiment-I (NDCX-I), and the conceptual designs of possible experiments on NDCX-I are investigated by making use of advanced numerical simulations. © *2011 American Institute of Physics*. [doi:10.1063/1.3557894]

I. INTRODUCTION

In the collective focusing scheme proposed by Robertson (hereafter referred to as a collective focusing lens), a weak magnetic lens provides strong focusing of an intense ion beam pulse carrying an equal amount of neutralizing electron background.[1–7] For instance, a solenoidal magnetic field of several hundred gauss can focus an intense neutralized ion beam within a short distance of several centimeters. Note that for a single-species non-neutral ion beam, a several Tesla magnetic field would be required to achieve the same focal length. The enhanced focusing in a collective focusing lens is provided by a strong self-electric field, which is produced by the collective dynamics of the neutralizing electrons.

The main features of the collective focusing lens can be summarized as follows. First, let us review the principles of operation of a conventional magnetic lens for the case of a single-species charged particle beam. Moving from a region of a zero magnetic field into the magnetic lens, a beam particle acquires azimuthal angular momentum as the magnetic flux through its orbit increases. As a result, a radial focusing $V\times B$ force acts on the beam particles inside the lens. For the case where the ion beam drags a neutralizing comoving electron background into the magnetic lens, the neutralizing electrons entering the lens experience much stronger magnetic focusing than the beam ions (due to the one over species mass scaling of the magnetic focusing force) and tend to build up a negative charge around the lens axis. As a result, a strong electrostatic ambipolar electric field develops to compensate for the large difference in the magnetic focusing forces acting on electrons and ions, which leads to a significant increase in the total focusing force acting on the ion beam (Fig. 1). Note that the neutralizing electrons should enter the lens from a region of a zero magnetic field in order to acquire the azimuthal angular momentum necessary for radial $V\times B$ magnetic focusing to occur inside the lens. Therefore, collective focusing will only occur if no background plasma or secondary electrons are present inside the lens. Otherwise, the rotating electrons comoving with the ion beam will be rapidly replaced by the "nonrotating" background plasma electrons inside the lens and the enhanced collective focusing will be suppressed.[6]

Many applications of ion-beam-driven high-energy density physics, including heavy-ion fusion and high-energy ion beam production from intense laser-matter interaction, require ion beam focusing and involve the presence of a neutralizing electron background. It is therefore of particular practical importance to investigate the feasibility of using a collective focusing lens for these applications. This would allow for the use of weak (several hundred Gauss) magnetic fields instead of a several Tesla conventional magnetic lens, thereby significantly facilitating the technical realization of intense ion beam focusing.

For instance, in the current design of a typical heavy-ion driver, a strong (several Tesla) magnetic solenoid is used to provide final transverse focusing of the ion beam as it leaves the drift section filled with a neutralizing background plasma.[8–10] Due to the strong space-charge self-fields of an intense ion beam pulse, a neutralizing plasma is also required inside the magnetic solenoid. Note that apart from the challenge of using a several Tesla magnetic solenoid, filling it with a background plasma provides additional technical challenges.[11] However, the use of the collective focusing concept can significantly simplify the technical realization of the beam final focus. Indeed, a neutralizing electron background can be dragged by the ion beam from the plasma that fills the magnetic-field-free drift section. The required mag-

[a]Present address: Lawrence Livermore National Laboratory, Livermore, CA 94550.

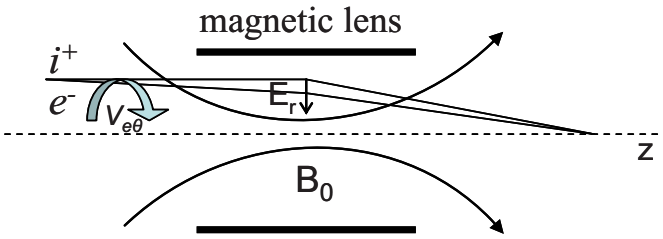

FIG. 1. (Color online) Schematic illustration of collective focusing lens configuration. Traversing the fall-off region of the solenoidal magnetic field, the comoving electrons acquire a fast rotation around the lens axis due to conservation of canonical angular momentum. As a result, a strong radial self-electric force is produced in order to balance the $V\times B$ magnetic force. This electric force has a dominant influence on the radial dynamics of the beam ions.

netic field of the final focus solenoid can be lowered to the range of several hundred gauss. Finally, a neutralizing plasma background is not required (should not be present) inside the final focus solenoid. As a practical example, in this paper, we present results of advanced numerical simulations demonstrating the feasibility of tight collective focusing of intense ion beams for the Neutralized Drift Compression Experiment-I (NDCX-I),[9] which is a heavy-ion driver for warm dense matter experiments.

A collective focusing lens can also be utilized in the laser generation of a high-energy ion beam, where the energetic ions are produced and accelerated by the interaction of an intense laser beam pulse with a thin foil.[12] In order to decrease the divergence of the ion beam, that is produced, a strong (several Tesla) focusing solenoidal magnetic field is used in some experiments.[13] However, along with the ions, a free-moving electron background is also produced, and therefore it is appealing to utilize the collective focusing concept for these applications as well.

The original analysis of a collective focusing lens was performed under the following assumptions. First, the neutralized ion beam was considered to be sufficiently dense, $\omega_{pe}\gg\omega_{ce}$, to maintain quasineutrality inside the magnetic solenoid.[1] Here, ω_{pe} and ω_{ce} are the electron plasma frequency and the electron cyclotron frequency, respectively. Second, perturbations in the applied solenoidal magnetic field due to the neutralized beam self-fields were assumed to be small. This condition can be expressed as $r_b\ll c/\omega_{pe}$, or equivalently, $I_b[\mathrm{kA}]\ll 4.25\beta_b$,[1,2] where r_b is the beam radius, I_b is the beam current, and β_b is the directed beam velocity normalized to the speed of light c. However, in many practical applications to high-energy density physics involving ion beam transport, the beam parameters may not be consistent with the above conditions. In particular, laser-produced, high-energy, short ion beam pulses are typically very dense, with the beam radius typically larger than the collisionless electron skin-depth, i.e., $r_b>c/\omega_{pe}$.[12,13] Also, propagation of a neutralized (by comoving electrons) ion beam along a strong solenoidal magnetic field with $\omega_{ce}>\omega_{pe}$ can occur both in a heavy-ion driver[9] and in the laser-production of collimated ion beams[13] when a conventional (several Tesla) magnetic lens is used for ion beam focusing. Therefore, the extension of previous theoretical models[1–7] to the cases where $\omega_{ce}>\omega_{pe}$ or $r_b>c/\omega_{pe}$ is of particular practical importance. In the present work, we investigate the operation of a collective focusing lens in these regimes, making use of advanced numerical simulations and reduced analytical models. In addition, the influence of the presence of a conducting wall surrounding the beam cross-section on the collective beam focusing is investigated.

The present paper is organized as follows. The original analysis of a collective focusing lens is summarized in Sec. II. Section III presents the results of advanced numerical simulations demonstrating the feasibility of tight collective focusing of intense ion beams for the NDCX-I. The effects of *non-neutral* collective focusing in a strong magnetic field, i.e., $\omega_{ce}>\omega_{pe}$, are investigated in Sec. IV, and the influence of the finite-radius conducting wall on the collective beam focusing is described in Sec. V. Finally, an analysis of collective focusing lens operation in the regime where the beam radius is comparable to or larger than the collisionless electron skin-depth, i.e., $r_b>c/\omega_{pe}$, is presented in Sec. VI.

II. THE COLLECTIVE FOCUSING LENS

In this section, we summarize the concept of a collective focusing lens proposed and experimentally tested by Robertson.[1] We consider a magnetic lens (magnetic solenoid) where a solenoidal magnetic field is nearly uniform inside the lens, $\mathbf{B}\cong B_0\hat{\mathbf{z}}$, and decreases rapidly to zero outside the lens. Note that the applied solenoidal magnetic field has a nonzero radial component B_r in the field fall-off region. When an ion beam carrying an equal amount of neutralizing electrons enters the lens along the axis of the solenoidal field, both the electron and the ion species acquire an angular momentum (Fig. 1). This occurs due to the $V_z\times B_r$ force, but can be conveniently calculated from the conservation of canonical angular momentum $P_{\theta\alpha}=m_\alpha r^2 d\theta_\alpha/dt-q_\alpha rA_\theta/c$. Here, (r,θ) corresponds to the cylindrical polar coordinates, A_θ is the azimuthal component of the magnetic field vector potential, $\nabla\times\mathbf{A}=\mathbf{B}$, m_α and q_α are the species mass and charge, respectively, and the subscripts $\alpha=e,i$ denote electrons or ions, respectively. Provided the neutralized beam enters the lens from a region of a zero magnetic field and does not significantly perturb the applied magnetic field of the lens, it follows that inside the lens, the angular rotation frequency is $\omega_\alpha\equiv d\theta_\alpha/dt=\Omega_\alpha/2$, where $\Omega_\alpha=q_\alpha B_0/m_\alpha c$, and initially nonrotating electrons and ions are assumed. The evolution of a particle's radial coordinate inside the lens is then governed by

$$\frac{d^2}{dt^2}r_\alpha+\frac{1}{4}r_\alpha\Omega_\alpha^2-\frac{q_\alpha}{m_\alpha}E_r=0. \tag{1}$$

Note that the second term on the left-hand-side of Eq. (1) corresponds to the difference between the centrifugal force $m_\alpha\Omega_\alpha^2 r/4$ and the $V_\theta\times B$ magnetic force $-m_\alpha\Omega_\alpha^2 r/2$.

In the original derivation for the case of a quasineutral ion beam, the identical radial motion of the electrons and the ions was assumed, i.e., $r_e(z,t)=r_i(z,t)$.[1] From Eq. (1), it therefore follows for the case of singly charged ions that

$$\frac{d^2}{dt^2}r_\alpha + \frac{1}{4}r_\alpha \Omega_e \Omega_i = 0, \tag{2}$$

and for the electric field we obtain $eE_r = -(m_i - m_e)\Omega_i \Omega_e r/4$, where $-e$ is the electron charge. Assuming $m_e \ll m_i$, we readily obtain that the strong ambipolar electric field that provides the enhanced collective focusing is given by

$$E_r = -m_e \Omega_e^2 \frac{r}{4e}. \tag{3}$$

Note that the electric field in Eq. (3) provides the balance between the magnetic $V_\theta \times B$ force, the centrifugal force, and the ambipolar electrostatic force acting on neutralizing electrons inside the lens. Furthermore, as pointed out in Ref. 14, the same results for the electric field [Eq. (3)] were obtained by Davidson in Ref. 15, where the possible equilibrium states for a plasma in a constant axial magnetic field were considered. Finally, a comprehensive analysis of the collective focusing lens including the thermal effects of the comoving electrons can be found in Refs. 4 and 5.

In the *thin*-lens limit, where the radial displacement of the beam particles within the lens is small, and the neutralized beam drifts to a focus outside the lens, the focal length of the collective focusing lens is given by[1]

$$L_f^{\text{coll}} = -v_b r_b/\Delta v_r \cong 4v_b^2/(\Omega_e \Omega_i L_s). \tag{4}$$

Here, v_b is the axial beam velocity, L_s is the length of the magnetic solenoid, r_b is the beam radius, and Δv_r is the radial velocity acquired within the lens. Note that the focal length of a "conventional" magnetic lens is given in the thin-lens approximation for a single-species ion beam by

$$L_f^m \cong 4v_b^2/(\Omega_i^2 L_s). \tag{5}$$

Equation (5) follows from Eq. (1), assuming that $E_r \cong 0$, provided the beam space-charge is weak or well-neutralized by a background plasma. Comparing Eqs. (4) and (5), it follows that for a given focal length, the magnetic field required for a neutralized beam is smaller by a factor of $\sqrt{m_i/m_e}$.

The quasineutrality condition, i.e., $|n_e - n_i| \ll n_i$, that has been assumed in the above analysis can be expressed in terms of practical system parameters by making use of Poisson's equation and Eq. (3). Here, n_e and n_i are the electron and ion number densities, respectively. After some straightforward algebra, it follows that the quasineutrality is maintained provided[1]

$$\omega_{pe}^2 \gg \tfrac{1}{2}\Omega_e^2. \tag{6}$$

It has also been assumed that the axial magnetic field perturbations due to the beam rotation are small. The azimuthal current density is primarily attributed to the electron rotation and is given inside the lens by $j_{e\theta} = -n_e e r \Omega_e/2$. Making use of Ampere's law, it is straightforward to show that the axial magnetic field perturbations are small provided[1]

$$\frac{1}{2}r_b \ll \frac{c}{\omega_{pe}}, \tag{7}$$

i.e., the beam radius is smaller than the collisionless electron skin-depth.

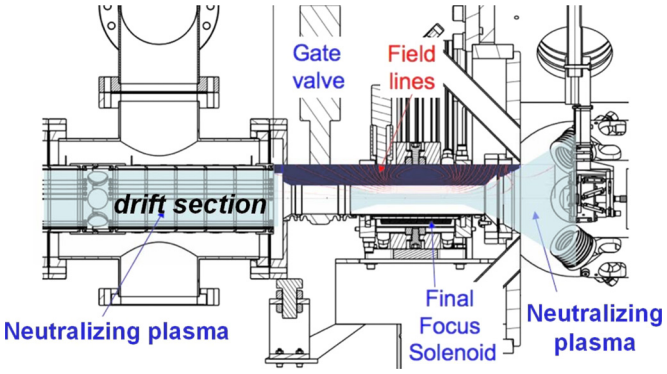

FIG. 2. (Color online) Schematic of the NDCX-I final focus section showing regions filled with neutralizing plasma. The neutralizing plasma inside the drift section is created by a ferroelectric plasma source (FEPS). The final focus solenoid is filled with a background plasma injected by four cathodic-arc plasma sources (only two are shown in the figure).

III. COLLECTIVE FOCUSING LENS FOR THE NDCX-I FINAL FOCUS

As noted earlier, it is appealing to make use of a collective focusing lens in the design of a heavy-ion driver final focus section. As a practical example, in this section, we consider the Neutralized Drift Compression Experiment-I (NDCX-I), which is designed to study energy deposition from a highly compressed intense ion beam pulse onto a target for warm dense matter physics studies.[9] To obtain a high-current, short ion beam pulse, a long, singly charged potassium ion bunch with directed energy of ~300 KeV and carrying a current of ~30 mA is matched into a solenoidal transport section, which controls the transverse beam envelope. Upon leaving the transport section, the radially converging beam pulse (with beam radius, $r_b \sim 1$ cm) acquires a head-to-tail velocity tilt and enters a long drift section ($L_d \sim 2$ m) filled with a background plasma ($n_p \sim 10^{10}-10^{11}$ cm^{-3}). The background plasma neutralizes the beam space-charge, and therefore nearly ballistic (field-free) simultaneous longitudinal and transverse compression occurs inside the drift section. In the present configuration of the NDCX-I device, final transverse focusing is then provided by a strong magnetic lens with magnetic field $B_s \sim 8$ T, and length $l_s \sim 10$ cm, which is placed downstream of the beam line after the drift section (Fig. 2). In order to compensate for the strong space-charge forces of the compressed ion beam pulse, the final focus solenoid has to be filled with a neutralizing plasma as well. In the present design, four cathodic-arc plasma sources are used to inject plasma into the final focus solenoid. The sources are placed out of the line-of-sight of the beam line in order to avoid interaction with the ion beam and angled toward the axis of the final focus solenoid (Fig. 2). Here, we emphasize again that filling the strong magnetic solenoid with a neutralizing plasma is itself a challenging problem,[11] and providing improved neutralizing plasma background inside the final focus solenoid is still one of the critical problems in NDCX-I optimization.

The final beam focusing can be significantly facilitated by using the concept of a collective focusing lens, which

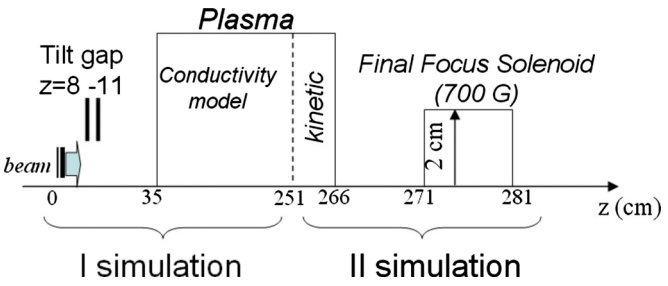

FIG. 3. (Color online) Schematic of the simulation configuration for NDCX-I using the LSP code.

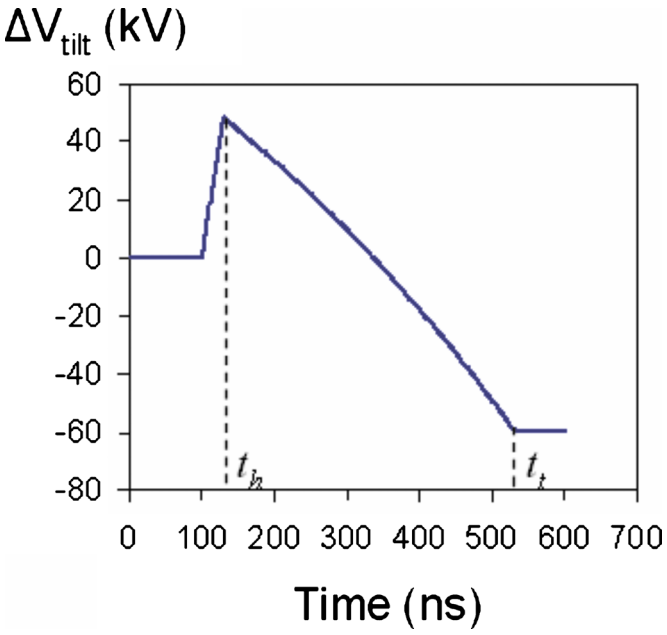

FIG. 4. (Color online) The idealized tilt-gap voltage waveform used in the numerical simulations.

requires minimum modifications to the current NDCX-I configuration. Indeed, in order to test the collective focusing, one needs to lower the final focus solenoid magnetic field from 8 T to several hundred gauss and turn off the cathodic-arc plasma sources. It is then expected that the beam will drag the required neutralizing comoving electrons from the background plasma that fills the drift section[16–21] and will experience strong collective focusing inside the magnetic solenoid.

In this section, we present the results of advanced numerical simulations demonstrating the feasibility of tight collective focusing of an intense ion beam pulse for NDCX-I. Note that the preliminary numerical simulations of the collective final focus in the NDCX-I were performed in Ref. 7, and focusing limitations due to possible heating of the comoving electrons during the transverse compression were discussed. However, those simulations did not take into account the effects of the beam's simultaneous, longitudinal and transverse, convergence and the pulse shaping inside the drift section. These effects are considered in the present analysis, and the feasibility of a tight collective final focus for the case of a more realistic beam distribution is demonstrated.

Figure 3 shows the schematic of the simulation configuration for NDCX-I. The singly charged beam ions ($Z_b=1$) are injected through the upstream boundary of the simulation domain at $z_{\rm inj}=0$. The injected beam current is $I_b=27$ mA, the directed energy of the K^+ beam ions is $E_b=300$ keV, the radial beam density profile is flat-top, with outer beam radius $r_{b0}=1.6$ cm, and the duration of the ion beam injection is $\tau_p\sim 500$ ns. Both the transverse and longitudinal beam temperatures are taken to be $T_b=0.094$ eV, and the initial radial convergence is $\Delta v_{r0}/v_b \equiv r_{b0}/L_{\rm conv}=0.02$. Note that this steep initial convergence angle, corresponding to a premature ballistic focus at $L_{\rm conv}=80$ cm, is taken to partially compensate for the radial beam divergence effects associated with the finite length of the tilt gap.[22] After injection, the beam propagates through the induction bunching module, where the time-dependent voltage shown in Fig. 4 is applied in the tilt gap between $z_{g1}=8$ cm and $z_{g2}=11$ cm. The beam then enters a long, $L_d=231$ cm, drift section filled with a neutralizing background plasma. A significant fraction of the simultaneous compression occurs inside the drift section. However, to provide the additional transverse collective focusing, a short, $L_s=10$ cm, final focus solenoid with radius $R_s=2$ cm is placed downstream of the beam line after the drift section. It is centered at $z_s=276$ cm, and the on-axis magnetic field inside the solenoid is $B_0=700$ G. Leaving the drift section, the beam is allowed to drag the comoving electron background from the background plasma, and a tight collective final focus is expected to be observed in the simulations.

The voltage ramp between the time instants $t_h=130$ ns and $t_t=530$ ns in Fig. 4 provides the longitudinal compression of only the $\tau_c\sim 400$ ns portion of the entire ion beam pulse; and the front part of the beam that propagates through the tilt gap during $t<t_h$ corresponds to the longitudinally uncompressed beam *prepulse*. Here, the subscripts h and t denote the head and tail of the beam pulse, respectively. The head of the compressing beam portion experiences a net decelerating electric force, and the tail experiences a net accelerating force. Thus, this part of the ion beam acquires a head-to-tail velocity tilt that causes the tail of the compressing beam portion to meet the head of the beam at the longitudinal focal plane. Note that the voltage ramp between t_h and t_t assumed in the simulations (Fig. 4) corresponds to the so-called idealized voltage waveform given by[22,23]

$$\Delta V_{\rm tilt}=\frac{m_b c^2}{2e}\left[\beta_b^2-\left(\frac{\beta_h}{1-c\beta_h(t-t_h)/L_f}\right)^2\right]. \tag{8}$$

Here, $\beta_b=v_b/c=0.004$ is the normalized directed beam velocity upstream of the tilt gap, $\beta_h=0.0037$ is the normalized head velocity of the compressing beam part, and $L_f=273$ cm corresponds to the drift distance to the ideal longitudinal focal plane. It is straightforward to show for ballistic compression of a cold beam that different longitudinal beam slices will come to the same focal plane at $z_{\rm foc}^{\rm id}=z_{g2}+L_f=284$ cm, provided their velocity is determined according to $m_b v_{\rm slice}^2(t)=m_b v_b^2-2e\Delta V_{\rm tilt}(t)$ at the tilt gap exit, i.e., $z=z_{g2}$.

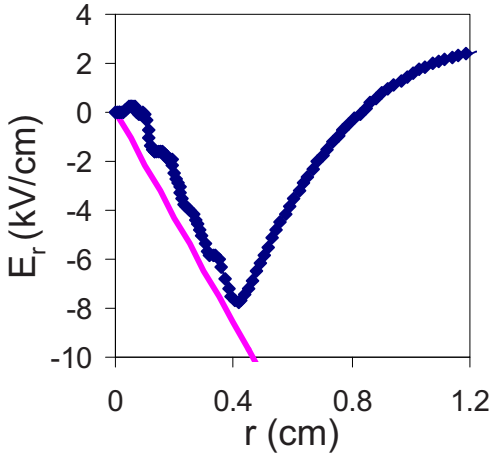

FIG. 5. (Color online) Results of the LSP simulations for the radial dependence of the radial electric field at the center of the final focus solenoid, $z=276$ cm, corresponding to $t=2535$ ns (blue dots). The analytical results in Eq. (3) are shown by the solid magenta line.

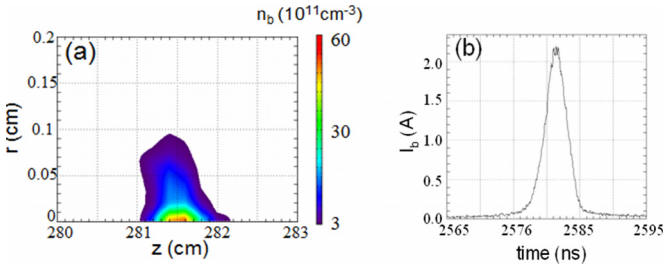

FIG. 6. (Color online) The ion beam parameters at the transverse focal plane. Shown are plots of (a) the ion beam density corresponding to $t=2580$ ns and (b) the time evolution of the ion beam current at the transverse focal plane corresponding to $z=281.6$ cm. The results are obtained using the LSP code.

It should be pointed out that the ideal simultaneous compression assuming perfect beam neutralization and the idealized voltage waveform [Eq. (8)] is still degraded by thermal effects, and the time-dependent effects of the longitudinal beam dynamics associated with a finite length of the tilt gap.[22,24–26] That is, traversing the finite-length tilt gap, the beam particles receive a time-dependent divergence angle.[22,25] Note again that the steep initial convergence angle is taken to partially compensate for this divergence. However, due to the time-dependent nature of the effect, simultaneous longitudinal and transverse beam compression is still degraded due to variations in the z-location of the transverse focal plane for different beam slices.[25,26] These finite-size tilt gap effects are adequately described by the present simulations, and the details of the tilt gap model can be found in Ref. 27. Among the deleterious technical effects that can limit simultaneous beam compression is a discrepancy between the ideal voltage waveform in Eq. (8) and the waveform generated by the induction bunching module in NDCX-I. This effect is considered in detail in Refs. 22 and 26, and is outside the scope of the present work.

It has previously been demonstrated that a dense background plasma with $n_p > n_b$ can provide a high degree of beam charge and current neutralization.[28] Furthermore, it can be shown that collective streaming processes do not have a significant influence on ion beam dynamics due to the thermal effects of the background plasma electrons. Therefore, it is appealing to use a fluid model for the background plasma, instead of a full kinetic description to simulate the ion beam pulse shaping during its simultaneous compression inside the long drift section. However, the kinetic effects of the comoving electrons are of particular importance for the collective focusing of the beam pulse. Accordingly, the entire simulation domain is divided into two parts. The simulation of the long upstream part, from $z=0$ to $z_L=251$ cm, utilizes a conductivity model for a background plasma, where a sufficiently high value of the conductivity is chosen to provide complete beam neutralization. The downstream part, from $z_L=251$ cm to $z_{\text{end}}=301$ cm, that includes a short downstream part of the drift section and the final focus section, is simulated by making use of a fully kinetic model for the background plasma electrons and ions. For this downstream simulation, we take the plasma density to be $n_p=10^{11}$ cm^{-3}, electron temperature $T_e=3$ eV, and the massive plasma ions are assumed to be cold. The beam ions are treated as a kinetic species throughout the entire simulation domain. We emphasize again that the use of a fluid model for most of the neutralizing plasma inside the drift section allows for a considerable reduction in the total computational time, and the details of the space-time resolution can be found in Ref. 27.

The results of the numerical simulations performed with the LSP code[29] are shown in Figs. 5 and 6. Figure 5 illustrates the strong radial focusing electric field generated by the beam inside the solenoid in accordance with the analytical predictions in Eq. (3). The corresponding "bell-shaped" profile of the ion beam density has characteristic radius of 0.5 cm, and peak number density of $\sim 2.5\times 10^{10}$ cm^{-3}. It is interesting to note that the radial electric field becomes positive outside the beam, implying incomplete global neutralization of the ion beam by the electron background. The incomplete global neutralization occurs due to the presence of the finite-radius conducting wall surrounding the beam cross-section and is described in detail in Sec. V. A plot of the beam density at the transverse focal plane is shown in Fig. 6(a). It is readily seen that a tight transverse collective focus with on-axis (peak) density of the compressed beam pulse $n_{\text{comp}}\approx 5.5\times 10^{12}$ cm^{-3} occurs in the simulations. The time evolution of the ion beam current at $z_{tf}=281.6$ cm corresponding to the transverse focal plane is shown in Fig. 6(b), which demonstrates strong $\sim$80X longitudinal compression, with peak current $I_p=2.2$ A, and a compressed ion beam pulse duration of a few nanoseconds. Note that the present illustrative simulations demonstrate the feasibility of a very tight collective focusing of the ion beam pulse in NDCX-I, and the compressed beam parameters are similar to the results of the simulations performed for the case where an 8 T final focus solenoid is used, and complete beam neutralization is assumed from the drift section entrance to the target plane.[9]

In conclusion, it is important to point out that the long prepulse part of the ion beam in the NDCX-I can produce a significant amount of the background electrons by preheating the target. Therefore, it may be important to remove those

electrons from the beam line. Otherwise, they may possibly leak into the final focus solenoid, thus reducing the collective focusing of the compressing part of the beam pulse. Note that the entire ion beam pulse undergoes simultaneous compression in the planned NDCX-II facility.[10,30] Therefore, the absence of the prepulse part of the ion beam makes the concept of final collective focusing even more attractive for the NDCX-II device. The proposed NDCX-II experiment is aimed at operating with a lithium ion beam (Li^+) at a higher energy, $E_b \approx 3$ MeV, and the final beam focusing will involve strong magnetic focusing by a final focus solenoid with $L_s \sim 10$ cm and $B_0 \sim 10$ T. Utilizing the collective focusing concept can allow for the use of a significantly less intense magnetic lens with $B_c = B_0(m_e/m_i)^{1/2} = 900$ G. However, note that in order to provide quasineutral collective focusing [see Eq. (6)], a beam density of $n_b[10^{10}\ \mathrm{cm}^{-3}] > 4.9 \times 10^{-6} B_c^2[\mathrm{G}] = 4 \times 10^{10}\ \mathrm{cm}^{-3}$ has to be reached at the exit of the drift section.

IV. NON-NEUTRAL COLLECTIVE FOCUSING

The original analysis of a collective focusing lens[1] assumed quasineutral compression, which is provided by the condition that the electron cyclotron frequency corresponding to the magnetic field inside the solenoid Ω_e is less than the electron plasma frequency of the incident neutralized beam, ω_{pe}^0 (Sec. II). However, it is of particular importance for several practical applications including the NDCX-I to investigate the collective focusing effect in a strong magnetic field with $\Omega_e > \omega_{pe}^0$. In this case, the quasineutrality condition inside the beam can break down, and it is important to determine the distribution of the radial electric field inside the beam, which is now supported by a pronounced charge separation.

In this section, we investigate the general features of non-neutral collective focusing in a strong magnetic field. We demonstrate for the case of sufficiently heavy and high-energy beam ions that the transverse dynamics of the comoving electron beam, which determines the radial electric field inside the ion beam, can be described as follows. When the magnetic field is weak, $\omega_{ce}(z) \ll \omega_{pe}^0$, the local density of the electron background follows that of the ion beam. The ion beam is well-neutralized, and a moderately strong magnetic $V \times B$ force, along with the centrifugal force acting on electrons, is balanced by an ambipolar (quasineutral) radial electric field [see Eq. (3)]. Here, $\omega_{ce}(z)$ denotes the local value of the electron cyclotron frequency. As the magnetic field strength increases to $\omega_{ce}(z) \sim \omega_{pe}^0$, the quasineutrality condition breaks down, $(n_e - Z_b n_i)/n_i \sim 1$, in order to provide a sufficiently strong radial electric field required for force balance on the electrons. Finally, with a further increase in the magnetic field strength, $\omega_{ce}(z) \gg \omega_{pe}^0$, strong charge separation occurs, $n_e \gg Z_b n_i$, and we demonstrate that the force balance on the electrons yields that the condition $\omega_{pe}(z) \approx \omega_{ce}(z)/\sqrt{2}$ is maintained during the electron compression. Here, $\omega_{pe}(z)$ is the local value of the electron plasma frequency.

It is interesting to note that the latter condition, i.e., $\omega_{pe}(z) \approx \omega_{ce}(z)/\sqrt{2}$, implies that the comoving electron beam

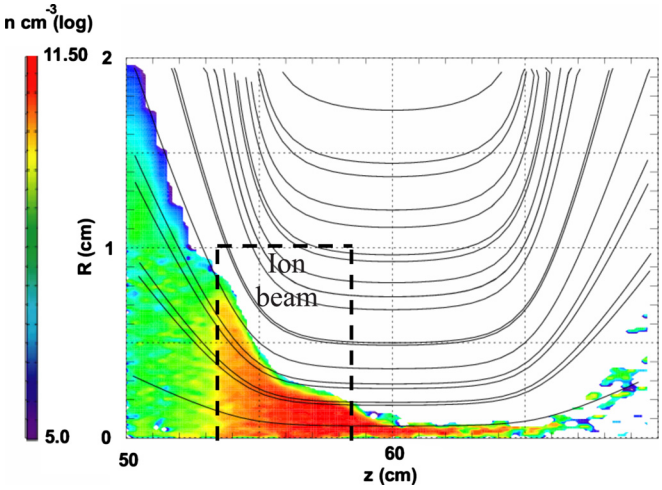

FIG. 7. (Color online) Steep compression of the neutralizing electron background in a strong solenoidal magnetic field. Shown is the plot of the electron density. The solid curves correspond to the magnetic field lines, and the bold dashed lines outline the ion beam. The neutralizing electrons are provided by a plasma layer with radius $R_p = 3.8$ cm located from $z = 0$ cm to $z = 15$ cm (see Fig. 9 for details). Steep electron compression across the magnetic field lines is evident for $z > 53$ cm. The maximum magnetic field at $z = 60$ cm corresponds to $\Omega_e = 5\omega_{pe}^0$, and infinitely massive beam ions are assumed. Other parameters of this LSP simulation are the same as in Figs. 9–11.

compression does not follow the magnetic field lines (Fig. 7). Indeed, the radius of a constant magnetic flux tube is given by $R_{\mathrm{flux}} \propto 1/\sqrt{\omega_{ce}}$, whereas the electron beam executes steeper compression with $R_e \propto 1/\omega_{ce}$ (assuming that the electron line density remains constant during the compression). This result is significantly different from the one that would be predicted by the "drift approximation",[31] which is often used for description of magnetized plasma flows, and would imply that the electron flow follows the magnetic field lines. The drift approximation assumes that charged particles exhibit fast rotation around magnetic field lines with thermal velocities, and their guiding centers slowly drift in the direction perpendicular to the magnetic field due to $E \times B$ drift, magnetic drifts, etc. However, for the present system, the strong electric field drags electrons across the magnetic field lines, and the azimuthal electron rotation around the lens axis ("guiding center" motion) is much faster than the gyrorotation attributed to the initial electron thermal velocity. Indeed, for the parameters considered in Sec. III, the energy of the azimuthal electron rotation provided by the strong electric field inside the solenoid, $m_e V_{e\theta}^2/2 = -eE_r r/2 = -e\int_0^r dr E$, corresponds to a few keV (see Fig. 5), whereas the initial thermal energy is only 3 eV. Therefore, the drift approximation is not valid for the present system, and the transverse dynamics of the electron flow is determined by the radial force balance, as described below.

We start the analysis by determining the conditions for a pronounced charge separation to occur inside an ion beam that carries an equal amount of electron background into a strong solenoidal magnetic field. Figure 8 illustrates a neutralized ion beam that propagates through an increasing solenoidal magnetic field, $B(z)$. For simplicity, we assume a uniform radial beam density distribution for the initial beam

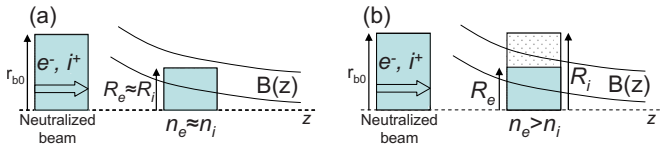

FIG. 8. (Color online) (a) Schematic illustration of a neutralized ion beam propagating along a strong solenoidal magnetic field with $\Omega_e > \omega_{pe}^0$. The two possible regimes of collective beam focusing correspond to (a) quasineutral collective focusing, where quasineutrality is maintained inside the beam during compression, and (b) non-neutral collective focusing associated with a pronounced build-up of negative charge near the beam axis.

state, with the flat-top density n_{b0} and outer beam radius r_{b0}. The ion beam is moving from a region of zero magnetic field, where its charge and current are completely neutralized by a comoving monoenergetic electron beam. We denote the electron cyclotron frequency corresponding to the maximum value of the magnetic field B_0 inside the solenoid by $\Omega_e \equiv eB_0/m_e c$, and assume that $\Omega_e > \omega_{pe}^0 = \sqrt{4\pi e^2 Z_b n_{b0}/m_e}$. Note that the condition $\Omega_e > \omega_{pe}^0$ itself does not necessarily imply that the quasineutrality is not maintained during transverse compression. Indeed, for the case of light, low-energy beam ions, and weak longitudinal gradients of the solenoidal magnetic field, quasineutrality will be maintained inside the beam, provided the increase in the electron plasma frequency due to the ion beam compression occurs more rapidly than the increase in the magnetic field, i.e., provided

$$\omega_{pe}^b(z) \gg \omega_{ce}(z). \tag{9}$$

Here, $\omega_{pe}^b = \sqrt{4\pi e^2 Z_b n_i(z)/m_e}$, $\omega_{ce} = eB(z)/m_e c$, and $n_i(z)$ is the local value of the ion beam density. For simplicity, we assume a short ion beam pulse with characteristic length that is much smaller than the longitudinal length-scale for variation of the magnetic field. The condition in Eq. (9) can then be expressed as

$$\frac{R_i(z)}{r_{b0}} \ll \frac{\omega_{pe}^0}{\omega_{ce}(z)}, \tag{10}$$

and the evolution of the ion beam outer radius $R_i(z)$ for the case of a quasineutral compression is given by

$$\frac{d^2 R_i}{dz^2} = -Z_b \frac{m_e}{m_b} \frac{R_i}{4} \frac{\omega_{ce}^2}{v_b^2}. \tag{11}$$

In the limit of a high-energy heavy-ion beam and steep magnetic field gradients, Eqs. (10) and (11) may not have a self-consistent solution. In this case, quasineutrality inside the beam is no longer maintained, and non-neutral collective focusing occurs.

In order to determine the transverse beam dynamics for the case of non-neutral collective focusing, one needs to investigate the distribution of the strong radial electric field inside the beam. For this purpose, we have performed advanced numerical simulations with the particle-in-cell code LSP, and a schematic of the present simulations is shown in Fig. 9. In an attempt to provide quiescent neutralization of the ion beam as it leaves the background plasma layer, cold plasma electrons are assumed, and a gradual decrease in the plasma density is introduced near the downstream end of the layer. That is, we take $n_p = 10^{11}$ cm^{-3} for $z < 12$ cm and then the plasma density is linearly decreased to zero over a distance of $l_{edge} = 8$ cm. We point out that the present numerical simulations demonstrate a high degree of beam charge neutralization as it leaves the plasma layer, and the velocity spread in the electron distribution is of order of the ion beam velocity (Fig. 10). A more detailed discussion describing the beam neutralization in the present simulations can be found in Ref. 27. The ion beam is injected from the left grounded conducting boundary of the simulation domain. To model the beam, we take $r_{b0} = 1$ cm, $n_{b0} = 10^{10}$ cm^{-3}, $Z_b = 1$, $\beta_b = 0.0042$, and $l_b \approx 5$ cm, and infinitely massive beam ions are assumed for simplicity. The maximum value of the magnetic field inside the focusing solenoid is $B_0 = 1600$ G, which corresponds to $\Omega_e = 5\omega_{pe}^0$, and the longitudinal profile of the on-axis magnetic field is shown in Fig. 9(b). Finally, a transverse cylindrical conducting boundary is present at $r_w = 3.8$ cm.

The results of the numerical simulations at an illustrative time $t = 500$ ns, when the beam is at the center of the magnetic solenoid, are shown in Fig. 11. As the comoving electrons enter the magnetic solenoid, the electrons acquire a strong azimuthal rotation due to conservation of canonical angular momentum [Fig. 11(a)]. The resulting $V \times B$ magnetic focusing force, along with the centrifugal force, is compensated by the strong radial self-electric field [Fig. 11(b)]. However, for the parameters considered here, $\omega_{pe}^b = \omega_{pe}^0 = \Omega_e/5$, the condition in Eq. (9) is violated, and a strong charge separation occurs in order to support the radial self-electric field [Fig. 11(c)]. Simulations show [Fig. 11(b)] that inside the electron beam, i.e., $r < R_e(z)$, the radial electric field is nearly linear, and is given by the electron force-balance equation

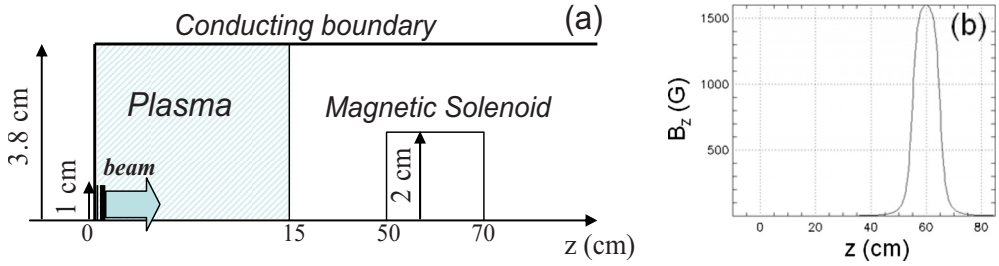

FIG. 9. (Color online) Collective focusing in a strong solenoidal magnetic field with $\Omega_e = 5\omega_{pe}^0$. (a) Schematic of the LSP simulations and (b) longitudinal profile of the applied axial magnetic field.

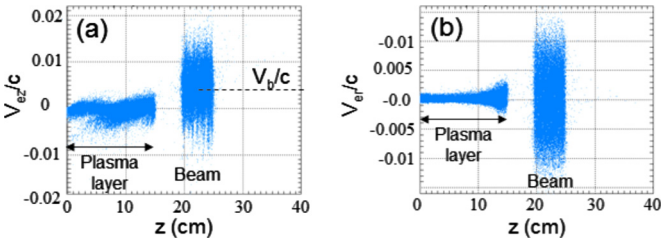

FIG. 10. (Color online) Thermal spreading of the comoving neutralizing electron beam at the time instant $t=200$ ns. Plots correspond to (a) longitudinal electron phase-space $(v_{ez}/c,z)$ and (b) the transverse electron velocity spreading $(v_{er}/c,z)$. The black dashed line in frame (a) illustrates the ion beam velocity. The velocity spreading of the initial cold background plasma electrons located inside the plasma layer from $z=-5$ cm to $z=15$ cm is attributed to electron heating due to beam-plasma interaction. The results are obtained using the LSP code.

$$E_r = -V_{e\theta}B_0/c + m_e V_{e\theta}^2/(er) = -m_e\omega_{ce}^2(z)r/4e. \tag{12}$$

Here, $R_e(z)$ is the characteristic outer radius of the electron beam, and $R_e<R_i$ [Fig. 11(c)]. For the case of a sufficiently long beam with $l_b \gg r_{b0}$, it follows from Eq. (12) that the electron beam density is uniform, and is specified by

$$\frac{1}{2}\frac{\omega_{ce}^2}{\omega_{pe}^2} = 1 - \frac{Z_b n_i}{n_e}, \tag{13}$$

where $\omega_{pe}^2(z)=4\pi e^2 n_e(z)/m_e$. For the case of strong non-neutral compression with $n_e \gg Z_b n_i$, we readily obtain that the condition $\omega_{pe}(z) \approx \omega_{ce}(z)/\sqrt{2}$ is maintained during the compression, which implies that electron compression does not follow the magnetic field lines. Finally, note that much better agreement between the analytical predictions in Eq. (12) and the results of the simulations in Fig. 11(b) is observed here, compared to the results presented in Sec. III (see Fig. 5). This is primarily due to the fact that in the present simulations (see Fig. 9), the magnetic solenoid is moved further downstream from the drift section in order to decrease the value of the fringe magnetic fields inside the plasma layer.

The nonlinear electric field in the region $R_e<r<R_i$ can be determined from Poisson's equation

$$\frac{1}{r}\frac{\partial}{\partial r}\left(r\frac{\partial\varphi}{\partial r}\right) = -4\pi Z_b e n_i(z), \tag{14}$$

which is to be solved subject to the boundary condition,

$$\left.\frac{\partial\varphi}{\partial r}\right|_{r=R_e(z)} = m_e\frac{\omega_{ce}^2(z)R_e(z)}{4e}. \tag{15}$$

In Eq. (14), the longitudinal derivatives have been neglected provided the beam is sufficiently long with $l_b \gg r_{b0}$. Note that the solution to Eqs. (14) and (15) is, in general, nonlinear even for a uniform ion beam density profile. As a result, the aberration effects caused by nonlinearities in the focusing electric field can significantly degrade the transverse focal spot.

In order to complete the description of the generated radial electric field, one needs to determine the evolution of the electron beam radius. The electron beam is being dragged into a strong solenoidal magnetic field by the intense ion beam. The rotational energy of the electrons and the electrostatic field energy arise from the directed energy of the ion beam; and the magnetic pressure force is globally balanced by the longitudinal variations of the electrostatic potential. However, the density profile of the comoving electron beam can still spread in the longitudinal direction as the beam propagates in the increasing magnetic field [Fig. 11(c)]. Furthermore, the presence of a finite-radius conducting wall surrounding the beam cross-section, which connects the neutralizing region (e.g., neutralizing plasma) and the region of a magnetic field (e.g., final focus solenoid), can provide additional reflection of outer-edge electrons, thereby reducing the total negative charge of the neutralizing electron beam (see Sec. V). Consistent with these facts, a fraction of the electron beam particles with negative values of longitudinal velocity has been observed in the simulations. For simplicity, in the present approximate estimate, we neglect the longitudinal broadening of the electron beam density profile and the finite-radius conducting wall effects, and assume that $n_e R_e^2 \sim n_{b0} r_{b0}^2$. Making use of this line-density conservation of the comoving electron beam, we obtain from Eq. (13) for the case of strong non-neutral compression, i.e., $n_e \gg Z_b n_i$, that

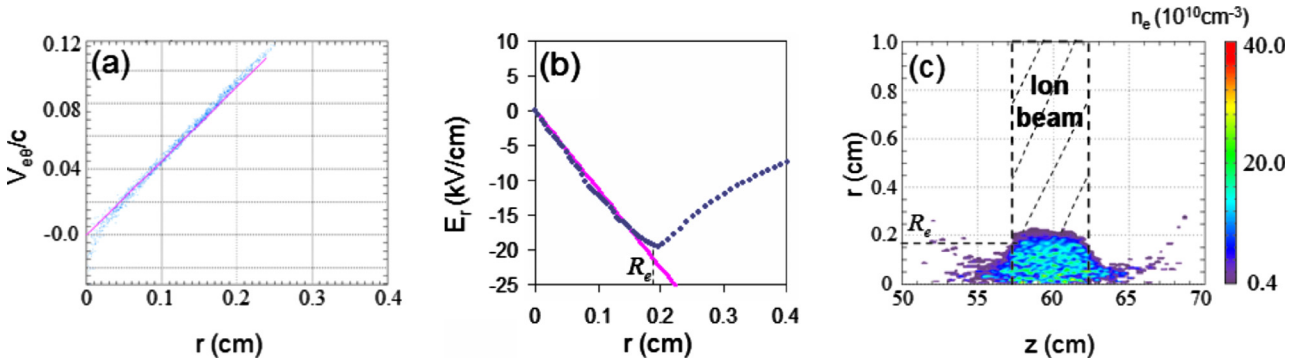

FIG. 11. (Color online) Non-neutral collective focusing. Shown are plots of (a) the electron phase-space $(V_{e\theta}/c,r)$, where the blue dots correspond to the results of the LSP simulations, and the estimate $V_{e\theta}=\omega_{ce}r/2$ is shown by the solid pink line; (b) radial dependence of the radial electric field at the center of the magnetic solenoid, $z=60$ cm, where the blue dots correspond to the results of the LSP simulations, and the analytical estimate in Eq. (12) is shown by the solid magenta line; and (c) electron density obtained in the LSP simulations. The dashed black lines in frame (c) outline the ion beam, and R_e corresponds to the characteristic electron beam radius. The time for the results shown in the figure corresponds to $t=500$ ns.

$$R_e(z) \sim \sqrt{2} r_{b0} \frac{\omega_{pe}^0}{\omega_{ce}(z)}. \tag{16}$$

Equations (14)–(16) together with Eq. (12) provide an approximate self-consistent estimate of the radial focusing electric field inside the ion beam. In conclusion, we discuss the validity of Eq. (12) that demonstrates the balance between the $V \times B$ magnetic focusing force, the centrifugal force, and the self-electric radial force acting on the background electrons. Equation (12) follows from the more general Eq. (1), provided the electron inertial term, i.e., the first term on the left-hand-side of Eq. (1), can be neglected. Making use of Eq. (16), it follows that the force-balance equation (12) is valid provided

$$l_m \gg v_b/\omega_{ce}, \tag{17}$$

where l_m is the characteristic length-scale for variations of the applied magnetic field.

V. EFFECTS OF THE CONDUCTING WALL ON COLLECTIVE FOCUSING

In this section, we investigate the collective focusing of an ion beam pulse, taking into account the effects of the finite-radius conducting wall surrounding the beam cross-section extending over the region of the beam initial neutralization (e.g., background plasma) and the magnetic field region (Fig. 9). We demonstrate that the presence of such a conducting boundary can lead to a lack of neutralizing electron background in the outer-edge region of the ion beam.

For simplicity, we again assume infinitely massive beam ions, and a flat-top radial density profile of the ion beam with the outer radius $R_i(z)=r_b=$const, and the number density $n_i(z)=n_b=$const. In Sec. IV, it has been shown for the case of an arbitrary ratio of ω_{ce}/ω_{pe} that the radial electric field inside the comoving electron beam is approximately linear in the radial coordinate r [see Eq. (12)]. Therefore, assuming that the beam is sufficiently long with $l_b \gg r_{b0}$ and neglecting by the longitudinal derivatives in Poisson's equation, it follows that the electron beam density can be approximated by a flat-top distribution with radius $R_e(R_e<r_b)$ and number density n_e. In what follows, we investigate a steady-state solution, in which a long coasting ion beam carrying a neutralizing electron background propagates from the neutralizing plasma into the magnetic solenoid. In particular, we estimate the degree of space-charge beam neutralization inside the magnetic solenoid.

Inspecting the motion of the on-axis (nonrotating) electrons, which follow the ion beam at an approximately constant velocity $V_{ez} \cong v_b$, it follows that the on-axis electrostatic potential is approximately constant downstream of the neutralizing plasma, i.e., $\varphi(r=0, z \geq z_p) \cong$ const. Here, z_p denotes the longitudinal coordinate of the downstream plasma boundary. Next, provided the neutralizing background plasma is sufficiently dense and cold, we neglect the potential variations (typical order of the electron temperature) inside the plasma, and therefore $\varphi(r, z \leq z_p) \cong \varphi_w =$const, where φ_w is the wall potential. It now readily follows that

$$\varphi(r=0, z \geq z_p) \cong \varphi(r=r_w, z \geq z_p) = 0, \tag{18}$$

where r_w is the conducting wall radius, and without the loss of generality, we assumed that the wall is grounded, i.e., $\varphi_w=0$. It is interesting to note that even if variations in the velocity of on-axis electrons around v_b are present (due to time-dependent effects, etc.), for many practical applications, the associated perturbations in the on-axis electrostatic potential are typically much smaller than the potential variations across the beam inside the magnetic solenoid, and therefore, the condition in Eq. (18) will still hold. For instance, for the parameters characteristic of NDCX-I, the beam velocity corresponds to the electron energy of a few eV, whereas the electrostatic potential variations across the beam are of the order of a few kV. The condition in Eq. (18) provides a constraint on the amount of the electron background that can be dragged into the solenoidal field.

We now calculate the electron line density at the center of the magnetic solenoid corresponding to the maximum electron cyclotron frequency Ω_e. From Eq. (12), it follows that inside the electron beam, the electrostatic potential is given by

$$\varphi(r) = \frac{m_e \Omega_e^2 r^2}{8e}, \quad 0 < r < R_e, \tag{19}$$

and making use of Poisson's equation for a long beam, $l_b \gg r_{b0}$, we obtain

$$\frac{n_e}{Z_b n_b} = 1 + \frac{\Omega_e^2}{2\Omega_p^2}, \tag{20}$$

where $\Omega_p^2 = 4\pi e^2 Z_b n_b / m_e$. For flat-top radial profiles of the ion and electron beam densities, it is straightforward to calculate the distribution of electrostatic potential in the region $R_e < r < r_w$, and show that the condition in Eq. (18) can be expressed as

$$\frac{m_e \Omega_e^2 R_e^2}{8e} - \pi Z_b n_b e (r_b^2 - R_e^2) + 2\pi e n_e R_e^2 \ln\frac{r_b}{R_e} - 2\pi e (Z_b n_b r_b^2 - n_e R_e^2) \ln\frac{r_w}{r_b} = 0. \tag{21}$$

Making use of Eq. (20), after some algebra, we obtain

$$\left(1 - \frac{N_b}{N_e}\right)\left(1 + 2\ln\frac{r_w}{r_b}\right) + \ln\left[\frac{N_b}{N_e}\left(1 + \frac{\Omega_e^2}{2\Omega_p^2}\right)\right] = 0, \tag{22}$$

where $N_b = \pi Z_b n_b r_b^2$ and $N_e = \pi n_e R_e^2$ are the ion and electron line densities, respectively. Equation (22) determines the *global* degree of the ion beam charge neutralization inside the magnetic solenoid for an arbitrary ratio of Ω_e/Ω_p. For the case of quasineutral beam propagation corresponding to $\Omega_e/\Omega_p \ll 1$, from Eq. (11), we obtain that the beam charge is well-neutralized,

$$\frac{N_b}{N_e} - 1 \cong \frac{\Omega_e^2}{4\Omega_p^2 \ln(r_w/r_b)} \ll 1, \tag{23}$$

provided the conducting wall is not in close proximity to the beam. The numerical solution to Eq. (22) as a function of $\Omega_e^2/2\Omega_p^2$ obtained for different values of r_w/r_b is shown in

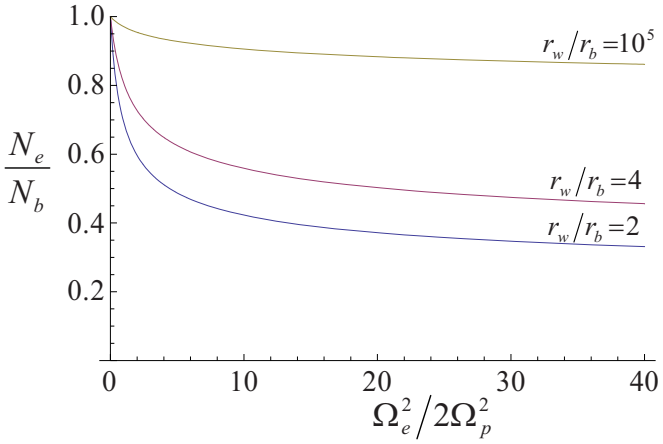

FIG. 12. (Color online) Numerical solutions to Eq. (22) demonstrating the global degree of ion beam charge neutralization inside the magnetic solenoid. The blue, purple, and brown curves correspond to $r_w/r_b=2$, $r_w/r_b=4$, and $r_w/r_b=10^5$, respectively.

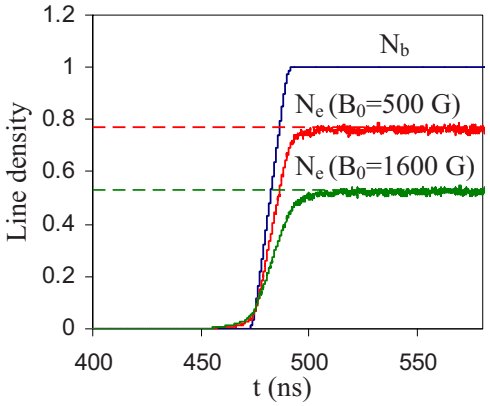

FIG. 13. (Color online) Time evolution of the ion and electron line densities at the center of the magnetic solenoid (z=60 cm) obtained using the LSP simulations. The blue curve shows the ion beam line density, and the red and green curves show the electron beam line density for the cases where the maximum values of the solenoidal magnetic field are B_0=500 G and B_0=1600 G, respectively. The corresponding horizontal dashed lines illustrate the solutions to Eq. (22) with r_w/r_b=3.8.

Fig. 12. It is readily seen that the total amount of neutralizing electrons that penetrate into the magnetic field decreases with an increase in the strength of the applied magnetic field.

The results of the analytical calculation in Eq. (22) have been found to be in a very good agreement with the results of the numerical simulations (Fig. 13). The parameters of these simulations are the same as in Sec. IV. The only difference is that the pulsed type of the beam injection used in Sec. IV has been replaced with a continuous injection in order to model a quasi-steady-state. Note that in the present numerical simulations, all conducting boundaries coincide with the domain boundaries, and no conducting surfaces are used to represent the boundaries of the magnetic solenoid. However, it is important to point out that by biasing the conducting surfaces of the solenoid relative to the chamber wall surrounding the neutralizing plasma, it is possible to control the amount of the neutralizing electrons inside the magnetic solenoid. Note that, in this case, the condition in Eq. (18) takes the form

$$\varphi(r=0,z>z_p)\cong\varphi(r=R_s,z>z_p)+\Delta V, \tag{24}$$

where ΔV is the voltage difference between the solenoid and the plasma chamber.

VI. COLLECTIVE FOCUSING OF A HIGH-INTENSITY ION BEAM WITH $r_b \geq c/\omega_{pe}$

As noted earlier, to assure small perturbations in the applied solenoidal magnetic field produced by the azimuthal component of the electron current, the beam radius has to be smaller than the collisionless electron skin-depth, i.e., $r_b \ll c/\omega_{pe}$. In this section, we present an analytical self-consistent calculation of the magnetic field perturbation, and discuss the collective focusing lens operation for arbitrary values of $r_b\omega_{pe}/c$.

Conservation of canonical angular momentum for the comoving electrons gives (Sec. II)

$$m_e V_{e\theta}=\frac{e}{c}A_\theta, \tag{25}$$

where $V_{e\theta}$ is the azimuthal component of the electron velocity, and initially nonrotating electrons are considered. Assuming that the beam radius is smaller than the beam pulse length, and smaller than the characteristic length-scale for variations of the applied solenoidal magnetic field, i.e., $r_b \ll l_b, l_m$, we obtain from Ampere's equation

$$\frac{\partial}{\partial r}\left(\frac{1}{r}\frac{\partial}{\partial r}(rA_\theta)\right)=\frac{4\pi}{c}en_eV_{e\theta}. \tag{26}$$

Furthermore, assuming for simplicity a uniform radial beam density profile with $n_e=n_i=n_b$ for $r\leq r_b$, and $n_e=n_i=0$ for $r>r_b$, Eq. (26) is to be solved subject to the boundary condition

$$\left[\frac{1}{r}\frac{\partial}{\partial r}(rA_\theta)\right]_{r=r_b}=B_s, \tag{27}$$

where B_s is the applied solenoidal magnetic field. Combining Eqs. (25) and (26) gives

$$\frac{\partial}{\partial \bar{r}}\left(\frac{1}{\bar{r}}\frac{\partial}{\partial \bar{r}}(\bar{r}A_\theta)\right)=A_\theta, \tag{28}$$

where $\bar{r}=r\omega_{pe}/c$. Solving Eqs. (27) and (28), it follows that the longitudinal component of the total magnetic field, i.e., $B_z=r^{-1}\partial(rA_\theta)/\partial r$, is given by

$$B_z=B_s\frac{I_0(r\omega_{pe}/c)}{I_0(r_b\omega_{pe}/c)}, \tag{29}$$

where $I_0(x)$ is the modified Bessel function of order zero. Plots of the total magnetic field $B_z(r)$, i.e., the sum of the beam-generated and the applied magnetic fields, for different values of $r_b\omega_{pe}/c$ are shown in Fig. 14. Note that attenuation of the longitudinal magnetic field results in a decrease in the focusing electric field since $E_r=-V_{e\theta}B_z/2c$. Furthermore, nonlinearities in the magnetic field profile provide aberra-

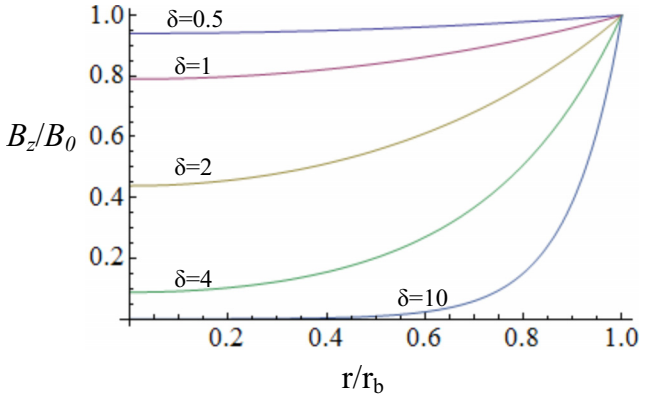

FIG. 14. (Color online) Radial dependence of the total magnetic field, i.e., the sum of the beam-induced and applied magnetic fields, for different values of $\delta=r_b\omega_{pe}/c$.

tions that can degrade the transverse focus. However, it is interesting to note that even for large values of $r_b\omega_{pe}/c$, the outer edge of the beam still experiences pronounced collective focusing (Fig. 14). It is, therefore, of great interest to carry out detailed self-consistent studies including the effects of the beam radial profile evolution, in order to estimate the applied magnetic field required to collimate or focus the intense ion beam.

Finally, we note that the effect of the diamagnetic screening of the focusing magnetic field by the comoving electron background can be important in applications where a solenoidal magnetic field is used to collimate the proton beam produced by interaction of an intense laser beam pulse with a thin foil.[13] Taking the beam current to be $I_b \sim 10^6$ A, and the proton beam energy at ~ 10 MeV, it follows that $\delta=r_b\omega_{pe}/c \approx 40$. Also, assuming the beam radius to be 1 cm, we obtain that the characteristic value of the magnetic field corresponding to $\omega_{ce}=\omega_{pe}^b=\sqrt{4\pi e^2 n_b/m_e}$ is $B \sim 3T$.

VII. CONCLUSIONS

In the present work, the collective focusing scheme in which a weak magnetic lens provides strong focusing of an intense ion beam pulse carrying an equal amount of neutralizing electron background has been investigated. This collective focusing can allow for the use of weak (several hundred Gauss) magnetic fields instead of the several Tesla fields used for a conventional magnetic lens, thereby significantly facilitating the technical realization of ion beam focusing for several applications to high-energy density physics. As a practical example, the feasibility of tight collective focusing of intense ion beams for the NDCX-I has been demonstrated by making use of advanced numerical simulations with the LSP code.

The original analysis of collective focusing,[1] assuming quasineutral transverse beam compression with $\omega_{ce} \ll \omega_{pe}$, has been extended to the case of non-neutral collective focusing, which can occur when the beam propagates in a strong solenoidal magnetic field with $\omega_{pe}^b=\sqrt{4\pi e^2 Z_b n_i/m_e} < \omega_{ce}$. This case can be of particular importance for several practical applications, including laser-production of high-energy ions, where a strong solenoidal magnetic field is used to collimate the divergent ion beam; and a heavy-ion fusion driver, where a strong magnetic solenoid is often used for final beam focusing. For the case of non-neutral collective focusing, the electron background executes a steeper compression compared to that of the beam ions, and as a result an excess of negative charge develops near the solenoidal axis. It has been shown for the case of strong non-neutral compression, with $n_e \gg Z_b n_i$ near the beam axis, that $\omega_{pe} \approx \omega_{ce}/\sqrt{2}$ is maintained inside the electron beam, and that the electron beam radius decreases approximately as $R_e \propto 1/\omega_{ce}$. The focusing radial electric field inside the electron beam $r<R_e$ is found to be linear with $E_r=-m_e\omega_{ce}^2(z)r/4e$. However, nonlinearities in the region $R_e<r<R_i$ cause aberrations, and can degrade the quality of the transverse ion beam focus.

In addition, the influence of a finite-radius conducting wall surrounding the beam cross-section on the collective focusing has been investigated for the case where the conducting wall connects the region of initial beam neutralization and the region with magnetic field. It has been shown for the case of quasineutral compression provided by $\omega_{ce} \ll \omega_{pe}$ that the presence of the wall does not degrade the charge neutralization of the ion beam as it propagates into the magnetic field region. However, with an increase in the magnetic field strength of the solenoid, $\omega_{ce} \geq \omega_{pe}$, the presence of a finite-radius conducting wall leads to a decrease in the global degree of beam charge neutralization. That is, the total amount (line density) of the neutralizing electron background inside the solenoid can become notably less than the total amount of ion beam charge.

Finally, the original analysis of collective focusing,[1] assuming small perturbations of the applied solenoidal magnetic field implied by $r_b \ll c/\omega_{pe}$, has been extended to the case of an arbitrary ratio of $\omega_{pe}r_b/c$. The perturbation in the solenoidal magnetic field produced by the azimuthal component of the electron beam current has been calculated self-consistently, and nonlinearities in the total magnetic field along with the significant suppression of the applied magnetic field have been demonstrated for $r_b \geq c/\omega_{pe}$. However, it has been found that even for large values of $r_b\omega_{pe}/c$, the outer edge of the ion beam pulse still experiences efficient collective focusing.

ACKNOWLEDGMENTS

The authors are grateful to E. P. Lee for pointing out the effect of the finite-radius conducting wall surrounding the beam cross section.

This research was supported by the U.S. Department of Energy under Contract No. DE-AC02-76CH-O3073 with the Princeton Plasma Physics Laboratory.

[1] S. Robertson, Phys. Rev. Lett. **48**, 149 (1982).
[2] S. Robertson, Phys. Fluids **26**, 1129 (1983).
[3] G. A. Krafft, C. H. Kim, and L. Smith, IEEE Trans. Nucl. Sci. **32**, 2486 (1985).
[4] G. A. Krafft, Ph.D. thesis, UC Berkeley, 1986.
[5] S. Robertson, J. Appl. Phys. **59**, 1765 (1986).
[6] R. Kraft, B. Kusse, and J. Moschella, Phys. Fluids **30**, 245 (1987).
[7] M. Dorf, I. D. Kaganovich, E. A. Startsev, and R. C. Davidson, Proceed-

ings of the 2010 International Accelerator Conference, Kyoto, Japan, 2010, p. 4635.

[8]S. S. Yu, R. P. Abbott, R. O. Bangerter, J. J. Barnard, R. J. Briggs, D. Callahan, C. M. Celata, R. C. Davidson, C. S. Debonnel, S. Eylon, A. Faltens, A. Friedman, D. P. Grote, P. Heitzenroeder, E. Henestroza, I. Kaganovich, J. W. Kwan, J. F. Latkowski, E. P. Lee, B. G. Logan, P. F. Peterson, D. Rose, P. K. Roy, G.-L. Sabbi, P. A. Seidl, W. M. Sharp, and D. R. Welch, Nucl. Instrum. Methods Phys. Res. A **544**, 294 (2005).

[9]P. A. Seidl, A. Anders, F. M. Bieniosek, J. J. Barnard, J. Calanog, A. X. Chen, R. H. Cohen, J. E. Coleman, M. Dorf, E. P. Gilson, D. P. Grote, J. Y. Jung, M. Leitner, S. M. Lidia, B. G. Logan, P. Ni, P. K. Roy, K. VandenBogert, W. L. Waldron, and D. R. Welch, Nucl. Instrum. Methods Phys. Res. A **606**, 75 (2009).

[10]A. Friedman, J. J. Barnard, R. H. Cohen, D. P. Grote, S. M. Lund, W. M. Sharp, A. Faltens, E. Henestroza, J.-Y. Jung, J. W. Kwan, E. P. Lee, M. A. Leitner, B. G. Logan, J.-L. Vay, W. L. Waldron, R. C. Davidson, M. Dorf, E. P. Gilson, and I. D. Kaganovich, Phys. Plasmas **17**, 056704 (2010).

[11]P. K. Roy, P. A. Seidl, A. Anders, F. M. Bieniosek, J. E. Coleman, E. P. Gilson, W. Greenway, D. P. Grote, J. Y. Jung, M. Leitner, S. M. Lidia, B. G. Logan, A. B. Sefkow, W. L. Waldron, and D. R. Welch, Nucl. Instrum. Methods Phys. Res. A **606**, 22 (2009).

[12]R. A. Snavely, M. H. Key, S. P. Hatchett, T. E. Cowan, M. Roth, T. W. Phillips, M. A. Stoyer, E. A. Henry, T. C. Sangster, M. S. Singh, S. C. Wilks, A. MacKinnon, A. Offenberger, D. M. Pennington, K. Yasuike, A. B. Langdon, B. F. Lasinski, J. Johnson, M. D. Perry, and E. M. Campbell, Phys. Rev. Lett. **85**, 2945 (2000).

[13]K. Harres, I. Alber, A. Tauschwitz, V. Bagnoud, H. Daido, M. Günther, F. Nürnberg, A. Otten, M. Schollmeier, J. Schütrumpf, M. Tampo, and M. Roth, Phys. Plasmas **17**, 023107 (2010).

[14]D. B. Boercker, D. M. Sanders, J. Storer, and S. Falabella, J. Appl. Phys. **69**, 115 (1991).

[15]R. C. Davidson, Phys. Fluids **19**, 1189 (1976).

[16]S. Humphries, Jr., Appl. Phys. Lett. **32**, 792 (1978).

[17]S. Humphries, Jr., T. R. Lockner, J. W. Poukey, and J. P. Quintenz, Phys. Rev. Lett. **46**, 995 (1981).

[18]R. Kraft and B. Kusse, J. Appl. Phys. **61**, 2425 (1987).

[19]D. Callahan, Fusion Eng. Des. **32–33**, 441 (1996).

[20]D. R. Welch, D. V. Rose, W. M. Sharp, C. L. Olson, and S. S. Yu, Laser Part. Beams **20**, 621 (2002).

[21]W. M. Sharp, D. A. Callahan, M. Tabak, S. S. Yu, P. F. Peterson, D. V. Rose, and D. R. Welch, Nucl. Fusion **44**, S221 (2004).

[22]A. B. Sefkow, Ph.D. thesis, Princeton University, 2007.

[23]C. H. Kim and L. Smith, Part. Accel. **18**, 101 (1985).

[24]A. B. Sefkow and R. C. Davidson, Phys. Rev. ST Accel. Beams **10**, 100101 (2007).

[25]A. B. Sefkow, R. C. Davidson, E. P. Gilson, I. D. Kaganovich, A. Anders, J. Coleman, M. Letner, S. M. Lidia, P. K. Roy, P. A. Seidl, P. L. Waldron, S. S. Yu, and D. R. Welch, Phys. Plasmas **16**, 056701 (2009).

[26]I. D. Kaganovich, R. C. Davidson, M. Dorf, E. A. Startsev, A. B. Sefkow, J. J. Barnard, A. Friedman, E. P. Lee, S. M. Lidia, B. G. Logan, P. K. Roy, P. A. Seidl, and D. R. Welch, *Proceedings of the 2009 Particle Accelerator Conference*, Vancouver, Canada, 2009 (IEEE, Piscataway, NJ, 2009), p. 3090.

[27]M. Dorf, Ph.D. thesis, Princeton University, 2010.

[28]I. D. Kaganovich, R. C. Davidson, M. A. Dorf, E. A. Startsev, A. B. Sefkow, A. F. Friedman, and E. P. Lee, Phys. Plasmas **17**, 056703 (2010).

[29]LSP is a software product of ATK Mission Research, Albuquerque, NM 87110.

[30]A. Friedman, J. J. Barnard, R. J. Briggs, R. C. Davidson, M. Dorf, D. P. Grote, E. Henestroza, E. P. Lee, M. A. Leitner, B. G. Logan, A. B. Sefkow, W. M. Sharp, W. L. Waldron, D. R. Welch, and S. S. Yu, Nucl. Instrum. Methods Phys. Res. A **606**, 6 (2009).

[31]N. A. Krall and A. W. Trivelpiece, *Principles of Plasma Physics* (McGraw-Hill, New York, 1973).